

Oxidative addition of iodo-acetonitrile and of elemental halogens to $[\text{Pt}_3(\mu\text{-CO})_3(\text{PCy}_3)_3]$

Zoltán Béni,^a Renzo Ros,^{*b} Augusto Tassan,^b Rosario Scopelliti^a and Raymond Roulet^{*a}

^a Institute of Chemical Sciences and Engineering, Swiss Federal Institute of Technology, Lausanne, BCH, CH-1015, Lausanne, Switzerland. E-mail: raymond.roulet@epfl.ch

^b Dipartimento di Processi Chimici dell'Ingegneria, Università di Padova, Via Marzolo 9, I-35131, Padova, Italy

Received 4th October 2004, Accepted 12th November 2004

First published as an Advance Article on the web 30th November 2004

The reaction of $[\text{Pt}_3(\mu\text{-CO})_3(\text{PCy}_3)_3]$ (**1**) with one mole-equivalent of iodo-acetonitrile was quantitative at -70°C giving the oxidative addition product $[\text{Pt}_3(\mu\text{-CO})_3(\text{PCy}_3)_3(\text{I})(\text{CH}_2\text{CN})]$ (**2**). Fragmentation of **2** was observed in solution giving $[\text{Pt}_2\text{I}(\text{CH}_2\text{CN})(\text{CO})_2(\text{PCy}_3)_2]$ (**3**) which is the major product at room temperature if the starting cluster/reactant ratio is equal to or less than 1 to 1.5. Dimer **3** decomposes slowly in solution giving $[\text{Pt}_2\text{I}_2(\text{CO})_2(\text{PCy}_3)_2]$ (**4a**) and succinonitrile. Monomer $[\text{PtI}(\text{CH}_2\text{CN})(\text{CO})(\text{PCy}_3)]$ was the final product of the reaction when using excess of iodo-acetonitrile. The reactions of **1** with one mole-equivalent of halogens X_2 gave the new 44-electron clusters $[\text{Pt}_3\text{X}(\mu\text{-CO})_2(\mu\text{-X})(\text{PCy}_3)_3]$ ($\text{X} = \text{I}_2$ (**7a**) or Br_2 (**7b**)) by oxidative addition followed by substitution of CO by X^- . Fragmentation of **7a** and **7b** took place in solution when using one and a half mole-equivalents of X_2 giving dimers **4a** and $[\text{Pt}_2\text{Br}_2(\text{CO})_2(\text{PCy}_3)_2]$ (**4b**) as well as $[\text{Pt}_2\text{X}_2(\mu\text{-X})_2(\text{CO})_2(\text{PCy}_3)_2]$. Monomers *cis*- $[\text{PtX}_2(\text{CO})(\text{PCy}_3)]$ were the final products of the reaction of **1** with excess of halogens. Insertion of SnCl_2 was observed into the Pt–Pt bond but not into the Pt–X bond, when equimolar amounts of $\text{SnCl}_2 \cdot 2\text{H}_2\text{O}$ were added to a solution of **4a** or its chloro-analogue giving $[\text{Pt}_2\text{X}_2(\mu\text{-SnCl}_2)(\text{CO})_2(\text{PCy}_3)_2]$. The Pt(I) dimers have unusually small $J(\text{Pt}–\text{Pt})$ values as observed by ^{195}Pt NMR and calculated by DFT. These values showed periodic changes comparing **4a** and its analogues with other halides and mixed halide dimers.

Introduction

Oxidative addition reactions involving mononuclear platinum complexes are widely studied since they are elementary steps in some catalytic cycles.^{1–4} In contrast not much is known on how platinum clusters act in this type of reaction.^{5–7} Continuing a study of the reactivity of triangulo phosphino-carbonyl platinum clusters,^{8–12} we report here on reactions with the electrophilic reagents iodo-acetonitrile and elemental halogens. Iodo-acetonitrile was chosen for being more reactive than methyl iodide which reacts extremely slowly at low temperature with $[\text{Pt}_3(\mu\text{-CO})_3(\text{PCy}_3)_3]$ (**1**). It is already known that elemental halogens react readily with clusters isostructural with **1** giving Pt(I) dimers and Pt(II) monomers,^{13,14} but no adduct complex having an intact Pt triangle has been reported so far. We investigated the reactions of **1** with I_2 and Br_2 targeting these clusters and the synthesis of $[\text{Pt}_2\text{I}_2(\text{CO})_2(\text{PCy}_3)_2]$ (**4a**) which was observed as a decomposition product of $[\text{Pt}_2\text{I}(\text{CH}_2\text{CN})(\text{CO})_2(\text{PCy}_3)_2]$ (**3**) formed in the reaction of **1** with iodo-acetonitrile.

The irregular behaviour of $J(\text{Pt}–\text{Pt})$ with respect to metal–metal distances was the object of a recent theoretical study.¹⁵ This study indicated that in Pt(I) dimers bearing CO and Cl ligands, σ interactions with CO ligands in axial positions were responsible for the reduced coupling constants. A DFT study was undertaken on model molecules of new Pt(I) dimers in order

to reproduce tendencies in the observed, unusually small $J(\text{Pt}–\text{Pt})$ values and to verify stereochemistries in solution.

Results and discussion

On the basis of X-ray analysis and *in situ* low temperature NMR and IR spectroscopic studies the following reaction schemes could be drawn for the reactions of $[\text{Pt}_3(\mu\text{-CO})_3(\text{PCy}_3)_3]$ (**1**) with iodo-acetonitrile (Fig. 1) and iodine (Fig. 2).

The reaction of **1** with one mole-equivalent iodo-acetonitrile is quantitative at -70°C , giving the oxidative addition product $[\text{Pt}_3(\mu\text{-CO})_3(\text{PCy}_3)_3(\text{I})(\text{CH}_2\text{CN})]$ (**2**). Upon warming, fragmentation occurred and mixtures of **2** and dimer $[\text{Pt}_2\text{I}(\text{CH}_2\text{CN})(\text{CO})_2(\text{PCy}_3)_2]$ (**3**) were observed, besides starting cluster **1**. Dimer **3** was the major product of the reaction at room temperature if the starting cluster/reactant ratio was equal to or less than 1 to 1.5. Upon standing in solution slow decomposition of **3** occurred giving the Pt(I) dimer $[\text{Pt}_2\text{I}_2(\text{CO})_2(\text{PCy}_3)_2]$ (**4a**) and succinonitrile. Excess of the electrophilic reagent converted **3** to Pt(II) monomer $[\text{PtI}(\text{CH}_2\text{CN})(\text{CO})(\text{PCy}_3)]$ (**5**), which was the final product of the reaction. An *in situ* NMR study indicated that **4a** slowly reacted with ICH_2CN and showed that this reaction was complete at 60°C giving *cis*- $[\text{PtI}_2(\text{CO})(\text{PCy}_3)]$ besides succinonitrile. Formation of the latter product suggests that scission of the Pt– CH_2CN bond is homolytic.

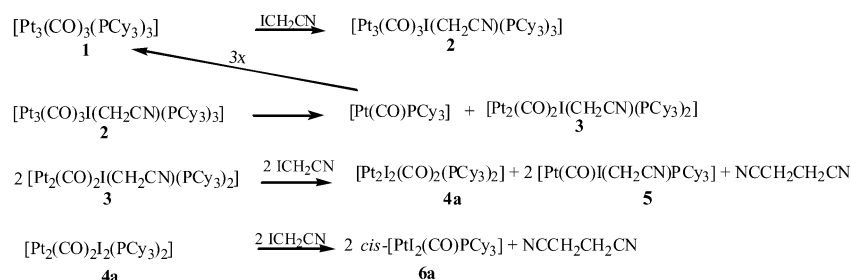


Fig. 1 Proposed reaction scheme for the reaction of **1** with iodo-acetonitrile.

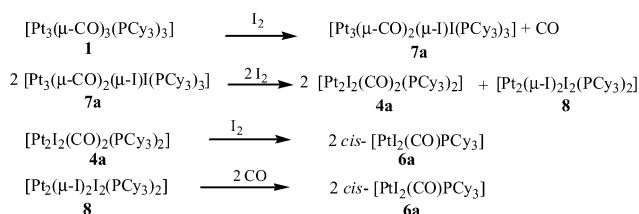


Fig. 2 Proposed reaction scheme for the reaction of **1** with iodine.

The reactions of **1** with one mole equivalent of elemental halogens (I_2 or Br_2) are more complex. After a possible oxidative addition step substitution of a CO ligand by a X^- takes place giving the new *triangulo*-clusters $[\text{Pt}_3\text{X}(\mu\text{-X})(\mu\text{-CO})_2(\text{PCy}_3)_3]$ ($\text{X} = \text{I}_2$ (**7a**) or Br_2 (**7b**)) bearing both bridging and terminal halide ligands. Besides these clusters, dimers **4a** or $[\text{Pt}_2\text{Br}_2(\text{CO})_2(\text{PCy}_3)_2]$ (**4b**) and the already known^{16–23} Pt(II) dimer $[\text{Pt}_2\text{X}_2(\mu\text{-X})_2(\text{PCy}_3)_2]$ ($\text{X} = \text{I}$, **8**) were observed as fragmentation products. Dimers **4a** or **4b** were the major products in dichloromethane when reacting **1** with one and a half mole equivalents of halogens. These dimers are analogues of complexes synthesized from clusters isostructural with **1** having phosphine ligands other than PCy_3 .^{14,24} The chloro-complex $[\text{Pt}_2\text{Cl}_2(\text{CO})_2(\text{PCy}_3)_2]$ (**4c**) was synthesized following the method reported by Mingos *et al.*²⁴ Dimers with mixed halide contents were formed by simple mixing of the corresponding dimers **4a**, **4b** or **4c**, indicating that intermolecular exchange of halide ligands is a fast process in solution. When using excess of halogens the final products were monomers *cis*- $[\text{PtX}_2(\text{CO})(\text{PCy}_3)]$ ($\text{X} = \text{I}$ (**6a**), Br (**6b**)), which are already known from literature.

Adducts $[\text{Pt}_3(\mu\text{-CO})_3(\text{PCy}_3)_3(\text{I})(\text{CH}_2\text{CN})]$ (**2**) and $[\text{Pt}_3\text{X}(\mu\text{-X})(\mu\text{-CO})_2(\text{PCy}_3)_3]$ ($\text{X} = \text{I}$ (**7a**), Br (**7b**))

The three adducts are 44-electron clusters. Adduct **2** is the first example of a cluster where a PtL_3 moiety is bonded to two PtL units. In contrast to our previous observation where the oxidative addition of the low polarity reagent Ph_3SnH converts the same starting cluster to a *cis* adduct, the two added ligands of **2** occupy opposite sides of the Pt_3 plane in an almost 180° arrangement. For mononuclear transition metal complexes, it has already been shown that similar reactions give *trans* (electrophilic reagents) and *cis* (low polarity reagents) products.⁴ The reactions with elementary halogens are more complex. After the oxidative addition substitution of one of the bridging CO by a $\mu\text{-X}$ ($\text{X} = \text{I}$ or Br) unit occurs which forces the remaining CO bridges to flip from the plane defined by the metal core to the other side compared to the two halide ligands. Cluster **2** is fairly stable in solution below 0°C , although no conditions were found where this complex was the sole product. In solution clusters **7a** or **7b** are thermally stable with respect to fragmentation up to 90°C .

Table 1 Selected distances (\AA) and angles ($^\circ$) of **2**

Pt(1)–Pt(2)	2.7369(6)	Pt(1)–I(1)	2.7289(10)
Pt(1)–Pt(3)	2.7340(6)	Pt(1)–C(1)	2.330(12)
Pt(2)–Pt(3)	2.6864(6)	Pt(2)–C(1)	1.925(12)
Pt(1)–P(1)	2.360(3)	Pt(2)–C(2)	2.055(12)
Pt(2)–P(2)	2.287(3)	Pt(3)–C(2)	2.159(12)
Pt(3)–P(3)	2.273(3)	Pt(1)–C(3)	2.288(11)
Pt(1)–C(4)	2.177(12)	Pt(3)–C(3)	1.983(12)
Pt(3)–Pt(1)–Pt(2)	58.819(16)	C(4)–Pt(1)–P(1)	94.0(3)
Pt(2)–Pt(3)–Pt(1)	60.645(16)	P(1)–Pt(1)–Pt(2)	152.90(7)
Pt(3)–Pt(2)–Pt(1)	60.536(16)	P(1)–Pt(1)–Pt(3)	145.77(7)
C(4)–Pt(1)–Pt(2)	92.1(3)	P(2)–Pt(2)–Pt(1)	155.71(8)
I(1)–Pt(1)–Pt(3)	77.14(2)	P(2)–Pt(2)–Pt(3)	143.76(8)
P(1)–Pt(1)–I(1)	94.31(8)	P(3)–Pt(3)–Pt(1)	152.20(8)
C(4)–Pt(1)–Pt(3)	97.2(3)	P(3)–Pt(3)–Pt(2)	146.85(8)
C(4)–Pt(1)–I(1)	171.3(3)	I(1)–Pt(1)–Pt(2)	79.38(2)
C(4)–Pt(1)–C(1)	84.0(4)	C(3)–Pt(3)–P(3)	98.4(3)

Complex **2** crystallized from toluene as a solvate of composition $[\text{Pt}_3(\mu\text{-CO})_3(\text{PCy}_3)_3(\text{I})(\text{CH}_2\text{CN})] \cdot 3.5\text{C}_6\text{H}_6$ (Fig. 3, left). X-Ray analysis showed that **2** is a Pt(II)Pt(0)Pt(0) cluster compound in which one Pt atom inserted into the iodo-alkyl bond of iodoacetonitrile. The metal triangle remains intact and is almost isosceles with Pt–Pt distances of 2.73 and 2.69 \AA (selected bond lengths and angles are listed in Table 1). These distances are very similar to the metal–metal bond lengths observed in the 44–electron $[\text{Pt}_3(\mu\text{-CO})_3(\text{PCy}_3)_4]$.²⁵

The phosphine ligands P2 and P3 remain almost coplanar with the metal triangle, with Pt–P distances of ~ 2.28 \AA . The Pt1–P1 distance is 0.05 \AA longer than the other two in accordance with the increased coordination number of the Pt1 center and is very similar to the corresponding bond lengths in the $[\text{Pt}_3\text{CO}]$ cluster. For the same reason the Pt–C(carbonyl) distances involving the Pt1 center are significantly elongated (2.29 and 2.33 \AA) compared to Pt2–C1 (1.93 \AA) and Pt3–C3 (1.98 \AA). The mean value of the Pt–CO distances is similar to that found in the starting cluster.^{25,26}

X-Ray analysis of **7a** (Fig. 3, right) shows that the Pt_3 triangle remains intact as well and is almost isosceles. The Pt–Pt distances (Table 2) are comparable with the $\text{L}_2\text{Pt}–\text{PtL}$ metal–metal bond lengths in the $[\text{Pt}_3\text{CO}]$ analogue of the starting cluster²⁵ or with the $\text{L}_3\text{Pt}–\text{PtL}$ distances in **2**. The increase in Pt–Pt bond lengths from **1** to **7a** is consistent with theoretical calculations on the transformation of a 42–electron to a 44–electron Pt cluster.^{27,28} The phosphine ligands remain coplanar with the metal core and the Pt–P bond lengths are similar to those found in the $[\text{Pt}_3\text{CO}]$ analogue of **1**.²⁵ Oxidative addition followed by substitution of a CO ligand by I^- has caused the remaining two carbonyl ligands to flip out from the metal plane and occupy opposite sides with respect to the two halide ligands. The Pt–P and Pt–C(carbonyl) distances involving the Pt1 centre (having the

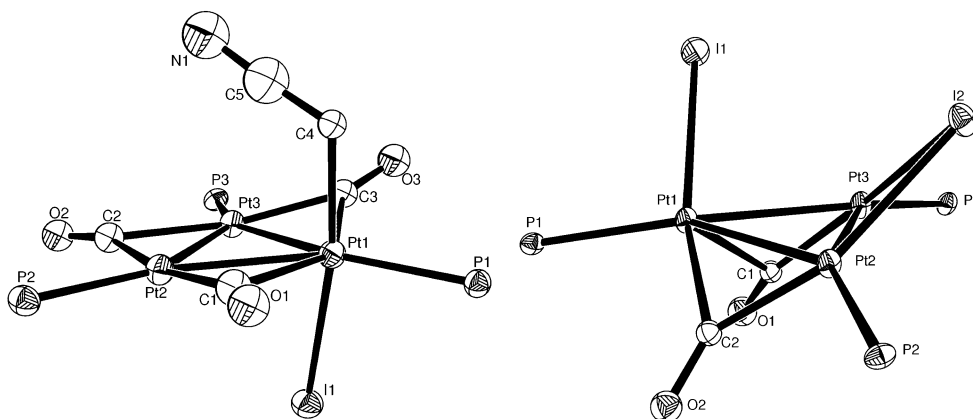


Fig. 3 ORTEP view of the core of **2** (left) and **7a** (right).

Table 2 Selected bond lengths (Å) and angles (°) of **7a**

Pt(1)–Pt(2)	2.7366(6)	Pt(2)–P(2)	2.258(3)
Pt(1)–Pt(3)	2.7231(7)	Pt(3)–P(3)	2.309(3)
Pt(2)–Pt(3)	2.7215(6)	Pt(1)–C(1)	2.174(12)
Pt(1)–I(1)	2.7524(11)	Pt(3)–C(1)	1.898(12)
Pt(2)–I(2)	2.7448(10)	Pt(1)–C(2)	2.034(13)
Pt(3)–I(2)	2.6748(10)	Pt(2)–C(2)	1.963(12)
Pt(1)–P(1)	2.328(3)	Pt(3)–Pt(1)–Pt(2)	59.796(17)
Pt(2)–Pt(3)–Pt(1)	60.349(17)	P(2)–Pt(2)–Pt(3)	151.31(9)
Pt(3)–Pt(2)–Pt(1)	59.854(17)	P(2)–Pt(2)–Pt(1)	145.24(9)
Pt(2)–Pt(1)–I(1)	114.14(3)	P(2)–Pt(2)–I(2)	108.92(9)
Pt(3)–Pt(1)–I(1)	77.83(3)	P(3)–Pt(3)–Pt(1)	147.27(8)
Pt(1)–Pt(2)–I(2)	103.60(3)	P(3)–Pt(3)–Pt(2)	148.08(8)
Pt(3)–Pt(2)–I(2)	58.59(2)	P(3)–Pt(3)–I(2)	105.09(9)
P(1)–Pt(1)–I(1)	97.29(9)	I(2)–Pt(3)–Pt(2)	61.14(2)
Pt(2)–I(2)–Pt(3)	60.27(6)	I(2)–Pt(3)–Pt(1)	105.88(3)
P(1)–Pt(1)–Pt(3)	156.66(8)	Pt(2)–C(2)–Pt(1)	86.4(5)
P(1)–Pt(1)–Pt(2)	139.93(8)	Pt(3)–C(1)–Pt(1)	83.6(5)

highest coordination number) are longer than the corresponding distances involving Pt2 and Pt3. The carbonyl and iodide ligands bridge asymmetrically the Pt–Pt edges (e.g. 2.17 (Pt1–C2) and 1.90 Å (Pt3–C2)). These asymmetries may be related with the fact that **7a** is stereochemically non-rigid in solution (see below).

Structures of **2** and **7a** (**7b**) in solution

The spectroscopic properties of **2** in solution (Table 3) are in accordance with its geometry in the solid state. Its IR spectrum presents two strong carbonyl stretching bands at 1872(b) and 1772(vs) cm^{-1} typical of bridging COs. In addition a weak absorbance at 2242 cm^{-1} indicates the presence of a terminal non-coordinated CN group.

Samples of **2** enriched to 99% ^{13}C CO consist of six isotopomers differing in the isotopic distribution of ^{195}Pt and all NMR spectra appear as superimpositions of subspectra. The ^{13}C NMR spectrum presents two chemically different CO environments centered at 224 (C3(1)) and 257 ppm (C2) with relative intensities 1 : 2, respectively. The chemical shift values confirm the bridging mode of the carbonyls, and the $\delta(\text{C}2)$ value is similar to the observed $\delta(\text{C})$ in **1** (259 ppm).¹¹ The most intense features in the spectrum have a triplet (C2) and a doublet of doublets (C3(1)) structure, due to $^2J(\text{C}–\text{C})$ and $^2J(\text{P}–\text{C})$ scalar couplings (Table 3). The $^1J(\text{Pt}–\text{C})$ and $^2J(\text{Pt}–\text{C})$ couplings involving the two distinct carbonyls differ slightly and are in accordance with the observed asymmetry of these carbonyls in the solid state. Thus e.g. the value of $^1J(\text{Pt1}–\text{C1}(3))$ (187 Hz) corresponding to bond lengths of about 2.3 Å are significantly smaller than those of $^1J(\text{Pt2}(3)–\text{C1}(3))$ which correspond to distances of about 2.0 Å. Due to inherent complexity, simulation of the ^{31}P NMR spectrum of

Table 4 Selected NMR data of **7a** (**7b**) at 90 °C (δ in ppm, J in Hz)

$\delta(\text{Pt})$	–4098 (–4029)	$^1J(\text{Pt}–\text{Pt})$	763
$\delta(\text{P})$	55.4 (50.5)	$^1J(\text{Pt}–\text{P})$	4805 (4814)
$\delta(\text{C})$	183	$^2J(\text{Pt}–\text{P})$	191 (202)
$^1J(\text{Pt}–\text{C})$	725	$^3J(\text{P}–\text{P})$	43.3 (43.0)

2 using the gNMR 4.1 software package did not completely converge, but a good fit was observed for the central peaks. The spectrum presents two distinct phosphine environments centered at 51.4 (P1) and 47.6 ppm (P2(3)). The one-bonded Pt–P coupling constants involving distinct phosphines differ markedly ($^1J(\text{Pt1}–\text{P1})$ 2589 Hz and $^1J(\text{Pt2}(3)–\text{P2}(3))$ 4474 Hz), which indicates that the oxidative addition affected mostly the Pt1 centre. All coupling constants involving only Pt2(3) and P2(3) are similar to those found in **1**, supporting again similar stereochemistries in solution and in the solid state. Two- and three-bonded coupling constant values are similar to the corresponding ones in **1b**. The ^{195}Pt spectrum of **2** presents broad signals and only chemical shift values are given in Table 3.

NMR measurements showed that clusters **7a** and **7b** are fluxional in solution. The terminal and bridging halide ligands and the two bridging COs are in fast exchange at the NMR scale. A limiting temperature for this dynamic process could not be reached down to –90 °C, only a significant line broadening was observed indicating that the dynamic process slowed down.

Accordingly, ^{31}P NMR spectra of **7a** in CD_2Cl_2 presented only one phosphine environment at 55.4 ppm (50.5 ppm in **7b**) with satellite peaks due to scalar coupling with three equivalent ^{195}Pt nuclei (Table 4), and with $^1J(\text{Pt}–\text{P})$ and $^2J(\text{Pt}–\text{P})$ values similar to those found in the starting cluster.²⁹

The ^{13}C NMR spectrum of **7a** is in accordance with the ^{31}P spectrum, as it showed a quartet central peak at 183 ppm with satellite peaks from coupling with three equivalent ^{195}Pt nuclei. ^{195}Pt NMR spectra showed a broad signal at –4090 ppm (–4029 ppm for **7b**). Raising the temperature resulted in narrower signals, but also induced a slow decomposition of **7a** (**b**) to **4a** (**b**) and **8**. At 90 °C, the ^{195}Pt NMR spectra presented a pseudo doublet of doublet of triplets in accordance with the ligand movement about the metal core and a proposed mechanism of the dynamic processes in solution is given in Fig. 4.

Pt(I) dimers [$\text{Pt}_2(\text{CO})_2(\text{PCy}_3)_2(\text{I})(\text{CH}_2\text{CN})$] (**3**) and [$\text{Pt}_2\text{X}_2(\text{CO})_2(\text{PCy}_3)_2$] ($\text{X} = \text{I}$ (**4a**), Br (**4b**), Cl (**4c**))

One and a half mole-equivalents of iodo-acetonitrile convert **1** to the asymmetric Pt(I) dimer [$\text{Pt}_2(\text{CO})_2(\text{PCy}_3)_2(\text{I})(\text{CH}_2\text{CN})$] (**3**). This dimer slowly decomposes upon standing in solution (even at –20 °C) giving back the starting cluster **1**, as well as **4a** and [$\text{PtI}(\text{CO})(\text{PCy}_3)(\text{CH}_2\text{CN})$] (**5**). Due to this decomposition

Table 3 Selected NMR data of **2** from gNMR simulation (δ in ppm, J in Hz)

$\delta(\text{C}2)$	257.2	$^1J(\text{Pt1}–\text{C1}(3))$	187	$^1J(\text{Pt1}–\text{P1})$	2589.8
$\delta(\text{C}3(1))$	224.4	$^1J(\text{Pt2}(3)–\text{C1}(3))$	1093	$^1J(\text{Pt2}(3)–\text{P2}(3))$	4474.2
$\delta(\text{P1})$	51.4	$^1J(\text{Pt2}(3)–\text{C}2)$	832.5	$^2J(\text{Pt2}(3)–\text{P1})$	385
$\delta(\text{P}2(3))$	47.6	$^2J(\text{Pt2}(3)–\text{C1}(3))$	26	$^2J(\text{Pt2}(3)–\text{P3}(2))$	412
$\delta(\text{Pt1})$	–4410	$^2J(\text{Pt1}–\text{C}2)$	38	$^2J(\text{Pt1}–\text{P2}(3))$	229
$\delta(\text{Pt}2(3))$	–4560	$^2J(\text{C}2–\text{C1}(3))$	30.1	$^3J(\text{P1}–\text{P2}(3))$	81
		$^2J(\text{C}–\text{P})$	~3–4	$^3J(\text{P2}–\text{P3})$	34.9

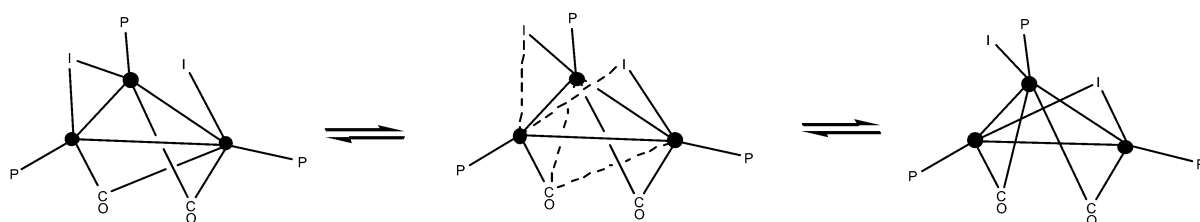
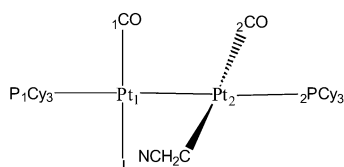
**Fig. 4** Proposed dynamic process of **7a** in solution.

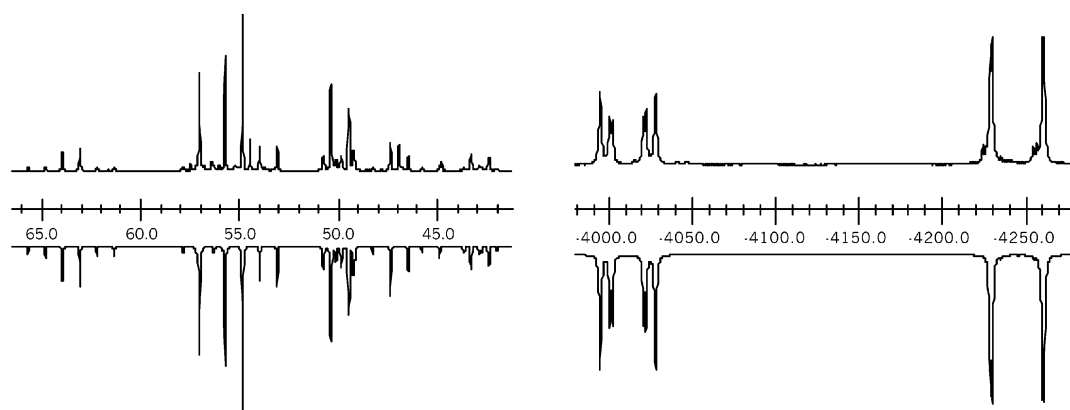
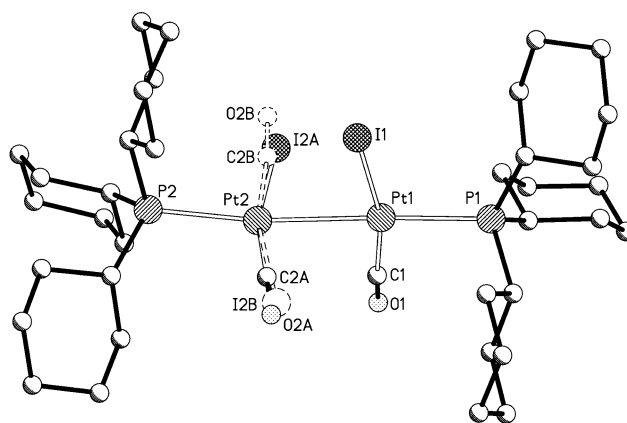
Table 5 NMR spectral data for **3** (δ in ppm, J in Hz)

$\delta(\text{C1})$	174.9	$^1J(\text{Pt1-C1})$	2009
$\delta(\text{C2})$	178.8	$^1J(\text{Pt2-C2})$	1260
$\delta(\text{P2})$	50.0	$^1J(\text{Pt1-P1})$	2675
$\delta(\text{P1})$	55.3	$^1J(\text{Pt2-P2})$	2300
$\delta(\text{Pt1})$	-4244	$^2J(\text{Pt2-P1})$	561
$\delta(\text{Pt2})$	-4010	$^2J(\text{Pt1-P2})$	115
$^1J(\text{Pt1-Pt2})$	166.5	$^3J(\text{P1-P2})$	144

all attempts to isolate **3** failed, hence only a structure in solution can be proposed (Fig. 5), which is based on the NMR data shown in Table 5 and on IR spectroscopic properties.

**Fig. 5** Proposed structure for dimer **3**.

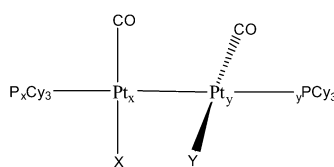
A satisfactory computer simulation of the ^{13}C NMR spectrum of **3** has been implemented on the basis of the superimposition of subspectra belonging to the four isotopomers differing in ^{195}Pt content. The ^{13}C NMR spectrum showed two chemically non-equivalent, terminal COs at 179 (C1) and 175 ppm (C2) with equal intensities, in accordance with the IR spectrum where two strong carbonyl absorbances were present at 2007 and 2035 cm^{-1} . In addition the latter spectrum presented a weak peak at 2205 cm^{-1} which could be attributed to a terminal, non-coordinated nitrile group. Computer simulation of the ^{31}P spectrum (Fig. 6, left) of **3** could be implemented with the support of the ^{195}Pt data. The ^{195}Pt NMR spectrum (Fig. 7, right) shows two well separated peaks appearing at -4244 ppm (similar to the δ observed in **4a**, see Table 6) and at -4010 ppm with expected $^1J(\text{Pt-P})$, $^2J(\text{Pt-P})$ and $^1J(\text{Pt-C})$ couplings. Comparison of corresponding $^1J(\text{Pt-C})$ and $^1J(\text{Pt-P})$ values of dimers **3** and **4a**, which share a common $[\text{Pt}(\text{CO})\text{I}(\text{PCy}_3)]$ unit, allowed the assignment of each Pt fragment of **3**, while the similarity of $^1J(\text{Pt-C})$ values in the $[\text{Pt}(\text{CO})(\text{PCy}_3)(\text{CH}_2\text{CN})]$ fragment of **3** and in **5** (1260 and 1120 Hz, respectively) suggested a similar *trans* arrangement of the CO and CH_2CN ligands about Pt2. The positive $^2J(\text{Pt1-Pt2})$ value of 564 Hz strongly suggests direct metal-metal interaction and that the two phosphine ligands occupy equivalent sites in a possibly linear P-Pt-Pt-P arrangement.³⁰ This suggestion was confirmed by a DFT calculation of coupling constants (see below) in model dimers. In contrast, $^2J(\text{Pt2-P1})$ is very small (115 Hz) as well as $^1J(\text{Pt1-Pt2})$ (166.5 Hz), but it is known that $^1J(\text{Pt-Pt})$ values are not always indicative of direct interaction between two platinum centers.^{15,31}

**Fig. 6** Observed and simulated ^{31}P (left) and ^{195}Pt (right) NMR spectra of **3** in d^8 -toluene at 283 K.**Fig. 7** Ball and stick representation of disordered dimer **4a**.

Dimer **3** decomposed upon standing in solution giving **4a** besides succinonitrile and monomer **5**. The presence of succinonitrile was confirmed by IR spectroscopy ($\nu(\text{CN})$ at 2254 cm^{-1}) and by a GC-MS measurement of a MeOH extract of the reaction residue.

Platinum(I) dimers similar to **4a** have already been reported.^{13,14,24,32,33} All these complexes contain terminally bonded halides. In these species the two Pt centres (having both square-planar geometry) associate almost perpendicularly with a direct metal-metal bond, as shown by the crystal structure of $[\text{Pt}_2\text{Cl}_2(\text{CO})_2(\text{P}^t\text{Bu}_2\text{Ph})_2]$ ¹⁴ and $[\text{Pt}_2\text{Cl}_2(\text{CO})_2(\text{PFc}_2\text{Ph})_2]$.²⁴ Treatment of **1** with 1.5 equivalents of elemental halogens led to the formation of the Pt(I) dimers $[\text{Pt}_2\text{X}_2(\text{CO})_2(\text{PCy}_3)_2]$ ($\text{X} = \text{I}$ **4a**, Br **4b**). The analogous complex containing chloride as ligand **4c** was synthesized by reduction of $[\text{Pt}(\text{COD})\text{Cl}_2]$ following the method developed by Mingos and co-workers.²⁴ Simple mixing of the corresponding dimers **4a**, **4b** or **4c** resulted in the immediate formation of the analogous complexes with mixed halide ligands.

Dimer **4a** crystallized from a toluene solution as a solvate, $[\text{Pt}_2\text{I}_2(\text{CO})_2(\text{PCy}_3)_2] \cdot 3.5\text{C}_7\text{H}_8$. X-Ray analysis (an ORTEP representation is shown in Fig. 7) showed that **4a** is isostructural with the complexes already cited.^{14,24} The dimer consists of two $[\text{PtI}(\text{CO})(\text{PCy}_3)]$ units (both of them close to planarity) linked *via* a direct metal-metal bond. The planes defined by the ligands about the two Pt centres are approximately perpendicular with a dihedral angle of 76.5° which is larger than the observed value of 66.5° in the related complex with a polyaromatic phosphine,²⁴ and the value of 70.1° observed in the dimer with $\text{P}^t\text{Bu}_2\text{Ph}$.¹⁴ This arrangement of the two planes renders the complex chiral. The iodide and the CO group around the Pt2 centre are disordered, in the sense that the iodide ligand occupies the position of the CO ligand in 20% of the molecules which are present in the crystal. The Pt1-Pt2 distance of 2.64 Å (see Table 7) is within the usual range (2.56–2.65) found for platinum(I) dimers,³⁴

Table 6 Selected NMR data of **4a** and its analogues


	X	Y	$^1J(\text{Pt}_x\text{-Pt}_y)$	$^1J(\text{Pt}_x\text{-P}_x)$	$^1J(\text{Pt}_y\text{-P}_y)$	$^2J(\text{Pt}_y\text{-P}_x)$	$^2J(\text{Pt}_x\text{-P}_y)$	$^3J(\text{P}_x\text{-P}_y)$
4a	I	I	0 ± 30	2617	2617	198	198	154
	I	Br	54	2628	2434	172	236	66
	I	Cl	110	2641	2318	177	291	79
4b	Br	Br	217	2415	2415	250	250	168
	Br	Cl	304	2419	2280	238	317	97
4c	Cl	Cl	535	2268	2268	344	344	181

Table 7 Selected bond lengths (Å) and angles (°) of **4a**

Pt(1)–Pt(2)	2.6374(5)	P(1)–Pt(1)–Pt(2)	177.83(4)	C(2A)–Pt(2)–P(2)	98.1(4)
Pt(1)–P(1)	2.3535(16)	P(2)–Pt(2)–Pt(1)	170.22(5)	C(2B)–Pt(2)–P(2)	93.6(8)
Pt(1)–I(1)	2.6353(7)	I(1)–Pt(1)–Pt(2)	83.242(18)	C(2A)–Pt(2)–I(2B)	3.4(4)
Pt(1)–C(1)	1.905(10)	I(2A)–Pt(2)–Pt(1)	84.27(2)	C(2B)–Pt(2)–I(2B)	164.0(8)
Pt(2)–P(2)	2.3440(17)	I(2B)–Pt(2)–Pt(1)	78.7(2)	C(2A)–Pt(2)–I(2A)	164.7(4)
Pt(2)–I(2A)	2.6246(11)	C(1)–Pt(1)–Pt(2)	83.1(2)	C(2B)–Pt(2)–I(2A)	11.2(10)
Pt(2)–I(2B)	2.604(6)	C(2A)–Pt(2)–Pt(1)	81.4(4)	P(2)–Pt(2)–I(2A)	96.92(5)
Pt(2)–C(2A)	1.845(8)	C(2B)–Pt(2)–Pt(1)	85.7(8)	P(2)–Pt(2)–I(2B)	101.1(2)
Pt(2)–C(2B)	1.856(8)	C(1)–Pt(1)–P(1)	96.1(2)	C(2A)–Pt(2)–C(2B)	165.9(9)
		C(1)–Pt(1)–I(1)	166.3(2)	I(2B)–Pt(2)–I(2A)	161.4(2)
		P(1)–Pt(1)–I(1)	97.60(4)		

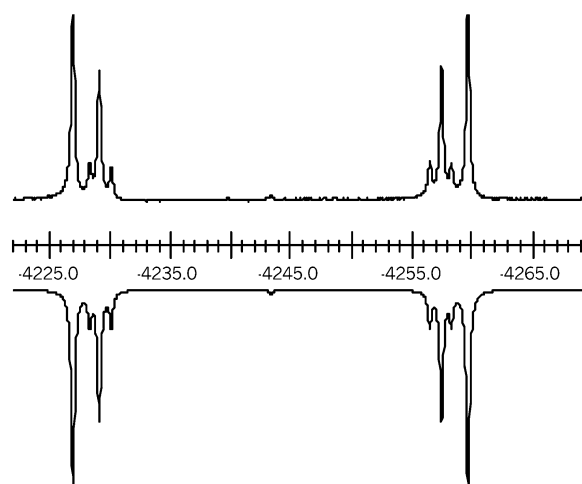
which is shorter than that observed in Pt(0) cluster complexes. The Pt–C(carbonyl) distances (1.90 and 1.85 Å) are very similar to those observed in isostructural complexes.

The IR spectrum of **4a** shows two strong CO bands at 2010 and 2030 cm^{-1} , indicative of terminally bonded CO groups. Analogous complexes showed similar absorption frequencies (around 2012 and 2035 cm^{-1}). An absorption band due to the Pt–X bond was observed at 172 and 216 cm^{-1} for **4a** and **4b**, respectively, which are typical of terminal Pt–X stretching frequencies.^{35,36}

The ^{31}P NMR spectra show a single resonance at 57.5 (**4a**), 56.1 (**4b**) and 55.6 ppm (**4c**), respectively, with satellites characteristic for two chemically but not magnetically equivalent phosphine environments. For complexes with mixed halide content the phosphine peaks are somewhat lower fielded. As expected, the spectra are the superimposition of subspectra related to the three isotopomers differing in ^{195}Pt content. Satisfactory computer simulations of these spectra have been implemented using gNMR 4.1 and have ascertained the assignments of all coupling constants (Table 6).

The ^{13}C NMR spectrum of **4a** confirmed the presence of terminally bonded CO ligands with a chemical shift value of 167.7 ppm, which is typical of this bonding mode. The ^{195}Pt spectra of **4a** (Fig. 8), **4b** or **4c** showed doublet of doublets as the most intense features centred at -4243.2 , -3998.7 and -3913.5 ppm, respectively.

The $^1J(\text{Pt}–\text{P})$ and $^1J(\text{Pt}–\text{C})$ values of 2617 and 1945 Hz, respectively, are similar to corresponding values in isostructural complexes.^{14,24} Complexes with other halides show the expected decrease in values of $^1J(\text{Pt}–\text{P})$ in accordance with the increased electronegativity of the halide and the decreased s-electron density of the Pt–P bond. The observed $^2J(\text{Pt}–\text{P})$ value (198 Hz) of **4a** is significantly smaller than that of the above referred complexes, or in **4b** (250 Hz) and in **4c** (344 Hz), but is close to the value of 219 Hz found in the Pt(I) dimer $[\text{Pt}_2\text{I}_2(\text{CO})_2(\text{P}^t\text{Bu}_2\text{Ph})_2]$.¹³ Furthermore $^1J(\text{Pt}–\text{Pt})$ coupling constants are small (0 ± 30 Hz in **4a**, 217 Hz in **4b** and 535 Hz in **4c**) compared to the estimated value of 748 Hz of the Mingos chloro-dimer containing polyaromatic phosphines.²⁴

**Fig. 8** Observed (top) and simulated (bottom) ^{195}Pt NMR spectra of **4a** in CD_2Cl_2 .

These small $^1J(\text{Pt}–\text{Pt})$ coupling constants may be rationalized on the basis of theoretical calculations due to Ziegler *et al.*¹⁵ Thus, the smaller value of $^1J(\text{Pt}–\text{Pt})$ observed when replacing a polyaromatic phosphine (748 Hz) by PCy_3 (535 Hz) is in accordance with the increased σ bonding ability of PCy_3 . The decrease of this coupling along the sequence $\text{Cl} > \text{Br} > \text{I}$ is in accordance with the relative σ bonding ability of these ligands and is in accordance with the trend observed in *e.g.* $[\text{Pt}_2\text{X}_4(\text{CO})_2]^{2-}$.³⁷

Three dynamic processes take place in solution. First, a rapid CO exchange was observed when a solution of **4a** was stirred under ^{13}C CO atmosphere. The lability of the CO ligands suggests that exchange may occur intermolecularly as well, but there is no direct evidence. Secondly, the rapid formation of the dimer complexes with mixed halide content by simple mixing of the corresponding dimers **4a**, **4b** or **4c** suggests that fast substitution of halide takes place in solution. This process probably occurs *via* the formation of a solvato-complex which liberates a small

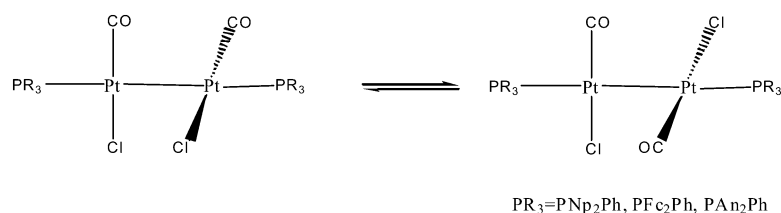


Fig. 9 Equilibrium of enantiomers.

quantity of halide. The third process is that already proposed by Mingos and co-workers²⁴ which occurs between enantiomers as presented in Fig. 9.

The suggested mechanism involves CO bridges in the transition state, based on a low temperature NMR study and MO calculation, which showed that the rotation about the Pt–Pt bond is not favoured since it has a high energy barrier of about 130 kJ mol⁻¹ (calculated for [Pt₂Cl₂(CO)₂(PH₃)₂]). Our low temperature ³¹P and ¹³C NMR measurements of complexes **4a**, **b** and **c** showed that all spectra in dichloromethane solution with or without the presence of a chiral environment (1(+)-*R*-camphor) were identical at each temperature. Changes in coupling constants showed the same tendency as that found by Mingos *et al.*²⁴ Coalescence points of the two lines belonging to diastereoisomers in the ³¹P NMR spectra are estimated to be -72 and -85 °C for **4a** and **4b**, respectively while in the case of **4c**, a limiting temperature could not be observed down to -105 °C. At these temperatures intermolecular substitution of halides still occurred. A mechanism of interconversion which also takes into account the observed intermolecular substitution of the halide ligands could start with the formation of a halide bridge and involve a nucleophilic attack of halide (Fig. 10).

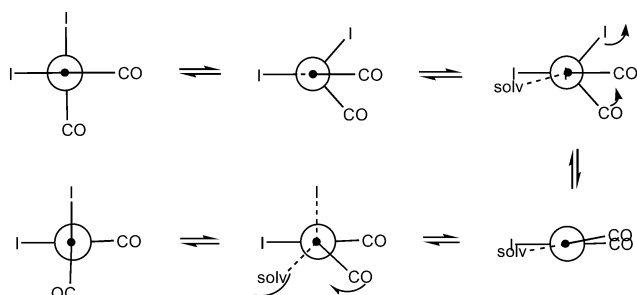


Fig. 10 Possible reaction mechanism for the interconversion of the enantiomers of **4a** presented with Newmann projections.

Dimers [Pt₂(μ-SnCl₂)(CO)₂(PCy₃)₂X₂] (X = I **9a** or Cl **9b**)

In order to get additional information about the low temperature behaviour of complexes similar to **4** but containing unambiguously terminal ligands, complexes **4a** and **4c** were reacted with SnCl₂·2H₂O, as we expected the formation of [Pt₂(SnCl₂X)₂(CO)₂(PCy₃)₂].

Surprisingly, the ¹¹⁹Sn NMR spectra (Fig. 11) of the products show bridging Sn units with two large ²J(¹¹⁹Sn–³¹P) (2050 and 2041 Hz in **9a** and **9b**, indicating *trans* Sn–P arrangement) and two relatively small ¹J(¹¹⁹Sn–¹⁹⁵Pt) coupling constants (6459 in **9a** and 7555 Hz in **9b**).

These spectral information exclude the formation of complexes with terminal SnCl₂X (X = I or Cl) groups. Conductimetric measurement in CH₃NO₂ showed that the complexes are neutral, which excludes substitution of halides by μ-SnCl₂. The IR spectrum indicated the presence of terminal COs, with stretching bands at 2050 and 2077 cm⁻¹.

The observed ³¹P and ¹⁹⁵Pt NMR spectra of **9a** and **9b** and the spectroscopic data (Table 8) were very similar to those of starting dimers **4a** and **4c**, indicating similar Pt(I) environments (only the observed ²J(Pt–P) value of 127 Hz (107 for **9b**) was somewhat

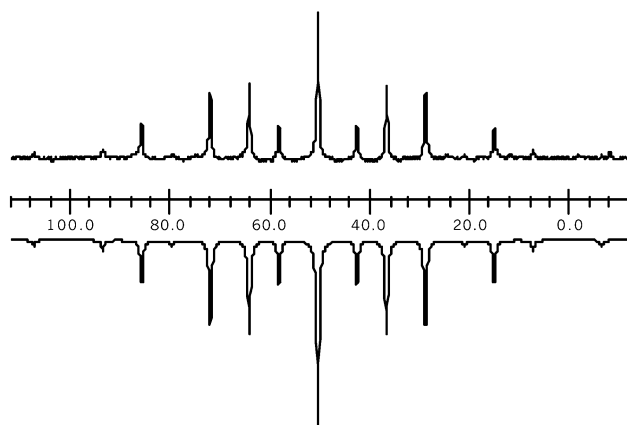


Fig. 11 Observed (top) and simulated (bottom) ¹¹⁹Sn spectra of complex **9a**.

Table 8 Selected coupling constants of complexes **8a** and **8b**

	9a	9b
δ _P	38.5	43.7
δ _{Pt}	-4655.7	-4272.5
δ _{Sn}	50.5	241.8
² J(Pt–Pt)	415	385
¹ J(Pt–P)	2163	1950
³ J(Pt–P)	104	128
⁴ J(P–P)	45	54
² J(Sn–P)	2050	2041
¹ J(Pt–Sn)	6458	7555

smaller). The observed ²J(Pt–P) values (415 in **9a** and 385 Hz in **9b**) were larger than those of **3** and **4a** (and somewhat smaller than that of **4c**).

All this information points towards the probable formation of [Pt₂(μ-SnCl₂)(CO)₂(PCy₃)₂X₂] (X = I for **9a** or Cl for **9b**). Pt₂(μ-Sn) groups have been prepared earlier by insertion of SnCl₂ into the Pt(I)–Pt(I) bond of [Pt₂X₄(CO)₂]²⁻,³⁸ by addition of Sn(acac)₂ to [(PPh₃)₂Pt(π-C₂H₄)],³⁹ or more recently by oxidative addition of tin(IV) halides to Pt(II) complexes.⁴⁰ It is also known that in the case of [Pt₂Cl₄(PEt₃)₂] insertion of the Sn(II) unit proceeds into a Pt–X bond⁴¹ rather than into the Pt–Pt bond. No single crystals of good quality were obtained because of slow decomposition of these complexes in solution. However X-ray analysis could ascertain the atomic connectivity of **9a** (Fig. 12).

DFT study of coupling constants in Pt(I) dimers

Dimers **3** and **4a** and its analogues show very small one-bonded Pt–Pt couplings reflecting small s-electron density between metallic centres and indicate that in the case of platinum there is no obvious correlation between bond lengths and nuclear spin–spin coupling constants. In the literature there is only one example (supported by a crystal structure) where the observed scalar coupling in a direct Pt–Pt bond is smaller than 200 Hz, *i.e.* *triangulo* [Pt₃(μ-CN^tBu)₃(CN^tBu)₃].⁴² Recently Ziegler and co-workers published a theoretical investigation of the irregular behaviour of Pt–Pt coupling constants.¹⁵ They studied three Pt(I) dimers, [Pt₂(CO)₆]²⁺ (¹J(Pt–Pt) = 551 Hz experimentally

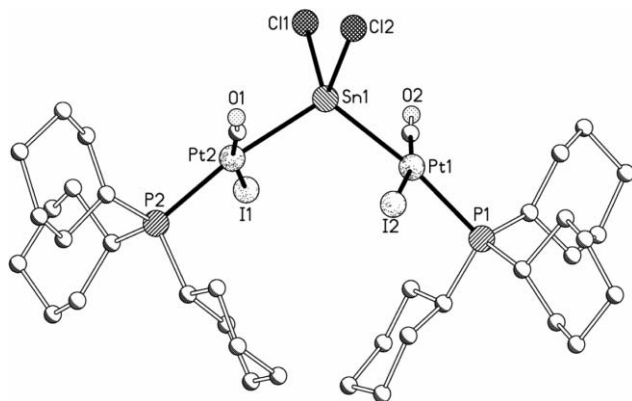


Fig. 12 Ball and stick representation of **9a** ($R = 0.120$).

observed and 874 Hz calculated), $[\text{Pt}_2\text{Cl}_4(\text{CO})_2]^{2-}$ (5250 Hz observed and 6397 Hz calculated, COs in equatorial positions, linear Cl–Pt–Pt–Cl arrangement) and its hypothetical isomer where the COs occupy axial positions (–963 Hz calculated). They found that σ interactions, particularly in the axial positions, are responsible for the reduced coupling constant in the hexacarbonyl dimer compared to the other dimer, and that π back donation of the COs has little effect. They showed that the relativistic effect has a great influence on the σ bonding capacity of Pt. The expected large magnitude of the Fermi contact contribution to coupling is to a large extent compensated by increasing σ interactions with axial CO ligands. Using these findings and comparing experimentally observed values of the Pt–Pt coupling constants in complexes **3**, **4a** and some analogues, one would expect that the reduction of metal–metal coupling

constants in complexes with axial COs or with axial phosphine ligands are comparable. This would be in accordance with the supposed small effect of π back donation of COs, which in itself is greater than that of phosphines, while σ interactions of these two types of ligands are similar. In order to verify these suggestions we investigated nuclear scalar couplings in model molecules which are analogues of **3**, **4a** and **4c** containing PMe_3 , to reduce the cost of the calculation.

Three model complexes were used for the calculation of nuclear coupling constants: $[\text{Pt}_2\text{I}(\text{CH}_2\text{CN})(\text{CO})_2(\text{PMe}_3)_2]$ (**3m**), $[\text{Pt}_2\text{I}_2(\text{CO})_2(\text{PMe}_3)_2]$ (**4am**) and $[\text{Pt}_2\text{Cl}_2(\text{CO})_2(\text{PMe}_3)_2]$ (**4cm**). The optimized geometry of **4am** was in good agreement with the solid state structure of **4a**, and the calculated geometry of **3m** has a smaller total bonding energy than that of a possible isomer of **3** having one phosphine ligand *trans* to the CH_2CN group (Fig. 13).

The calculated $^1J(\text{Pt–Pt})$ and $^2J(\text{Pt–P})$ values of **3m**, **4am** and **4cm**, using all electron TZP basis sets were overestimated while $^1J(\text{Pt–Pt})$ was underestimated (Table 9) compared to the corresponding experimental values, although comparing them to models with PH_3 as ligands they were largely improved. Only the calculated Pt–C coupling constants were in good agreement with the experimentally observed values. Unfortunately further increment of the size of the model molecules (using larger phosphines) was not possible with an acceptable increase of the cost of the calculations. Solvent effect has already been shown⁴³ to have a major role in the magnitude of metal–metal nuclear coupling constants in heterometallic Pt–Ti dimers, therefore computation of scalar couplings were repeated on **3m** and **4am**, applying the conductor like screening model (COSMO)^{44–46} of solvation. Using this solvation model improved significantly the quality of the calculated results (Table 9) compared to the

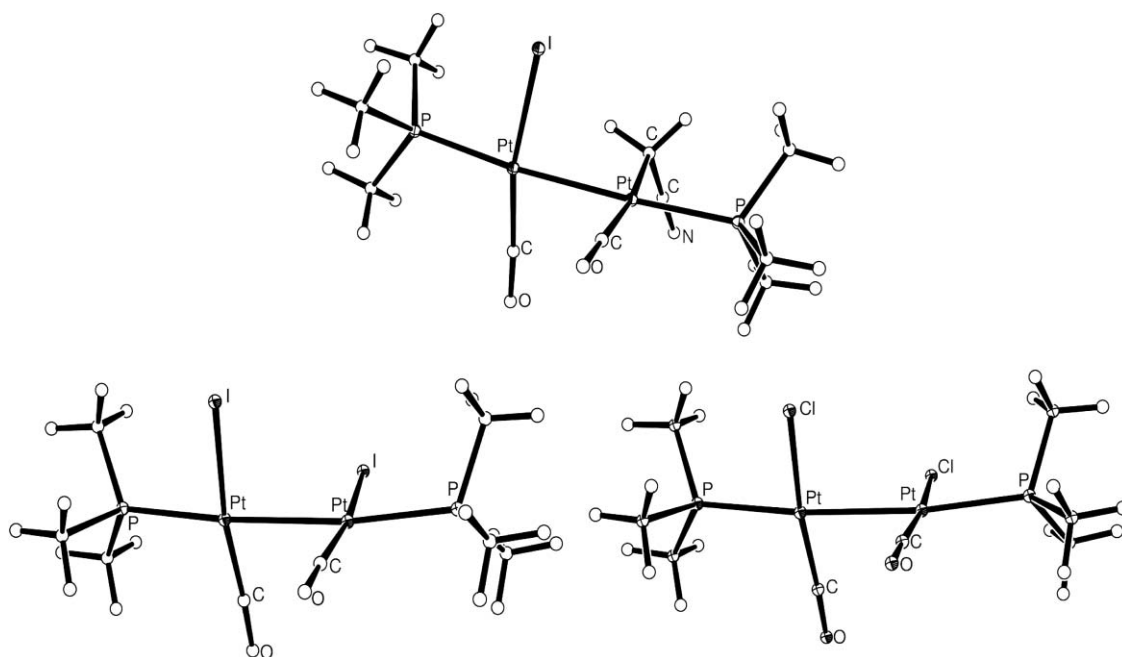


Fig. 13 Optimized geometries of model dimers **3m**, **4am** and **4cm**.

Table 9 Experimentally observed (for **4a**, **3** and **4c**) and calculated (full electron, COSMO) coupling constants for **4am**, **3m** and **4cm**

	Exp 4a	Exp 3	Exp 4c	Calc. 4am	Calc. 3m	Calc. 4cm	Calc. 4am COSMO	Calc. 3m COSMO
$^1J(\text{Pt1–Pt2})$	0	167	535	1094	1355	1695	863	1001
$^1J(\text{Pt1–P1})$	2617	2675	2268	1632	1530	1323	1709	1633
$^2J(\text{Pt1–P2})$	198	115	344	427	352	650	222	217
$^1J(\text{Pt1–C1})$	1945	2009	—	2065	2115	—	2198	2233
$^1J(\text{Pt2–P2})$	2617	2300	2268	1632	1468	—	1709	1513
$^2J(\text{Pt2–P1})$	198	561	344	427	837	—	222	585
$^1J(\text{Pt2–C2})$	1945	1260	—	2065	1396	—	2198	1475

Table 10 Differences in observed and calculated coupling constants (Hz)

	$\Delta^{\text{exp}} (J_3 - J_{4a})$	$\Delta^{\text{calc}} (J_{3m} - J_{4am})$	$\Delta^{\text{calc}} (J_{3m} - J_{4am})$ COSMO	$\Delta^{\text{exp}} (J_{4c} - J_{4a})$	$\Delta^{\text{calc}} (J_{4cm} - J_{4am})$
$^1J(\text{Pt1-Pt2})$	167	261	138	535	601
$^1J(\text{Pt1-P1})$	58	-102	-76	-349	-309
$^2J(\text{Pt1-P2})$	-83	-75	-4	146	223
$^1J(\text{Pt1-C1})$	34	50	36		
$^1J(\text{Pt2-P2})$	-317	-163	-196	-349	-309
$^2J(\text{Pt2-P1})$	363	410	363	146	223
$^1J(\text{Pt2-C2})$	-715	-669	-723		

previous calculations. Calculated $^1J(\text{Pt-Pt})$ and $^2J(\text{Pt-P})$ values decreased while $^1J(\text{Pt-P})$ and $^1J(\text{Pt-C})$ values increased. The numerical values of $^1J(\text{Pt-Pt})$ and $^1J(\text{Pt-P})$ are still not in good agreement with the experimental ones but $^1J(\text{Pt-C})$ and $^2J(\text{Pt-P})$ values are.

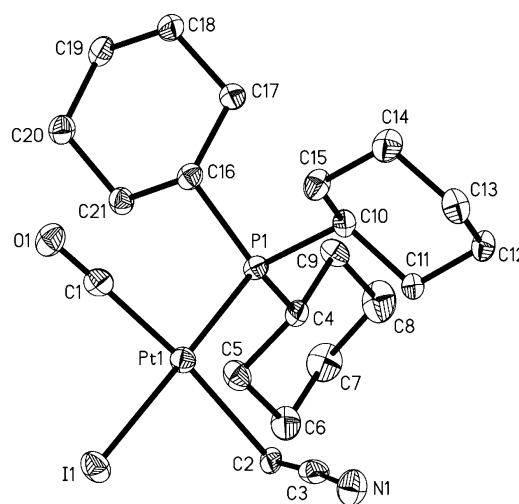
Comparison of differences between observed and calculated coupling constants (Table 10) show that both calculations (using COSMO or not) were able to reproduce trends in these values. Thus, for example, the calculations (not applying COSMO) predict the $^1J(\text{Pt-Pt})$ value to be smallest in **4am** and largest in **4cm**, which is indeed the case in the experimentally observed metal-metal coupling constants. The calculated large differences in the values of two different pairs $^2J(\text{Pt-P})$ and $^1J(\text{Pt-C})$ in **3m** fit well with the corresponding observed differences between these couplings in complex **3**. This confirms that the structure supposed for **3** based on NMR data is most probably right and indicates that the cyano-alkyl group is responsible for significant changes in these values.

In conclusion these calculations clearly showed that PH_3 fails to model PCy_3 in dimeric Pt complexes. The calculation confirmed the suggested structure of complex **3**. Trends in corresponding coupling constants were nicely reproduced with model systems containing PMe_3 as ligands, although the numerical values differed significantly from experimentally observed ones. These differences were probably due to the improper electronic description of these systems. Autsbach *et al.*¹⁵ have already shown that standard ADF basis sets are not flexible enough in the core region in the case of heavy elements such as platinum for calculating coupling constants. They suggested that one has to add steep basis functions with high exponents to reach the required flexibility. In the absence of such basis sets we had to settle for conventional ADF sets.

Monomers $[\text{Pt}(\text{CO})(\text{PCy}_3)(\text{CH}_2\text{CN})]$ (**5**), *cis*- $[\text{Pt}_2(\text{CO})(\text{PCy}_3)]$ (**6a**) and its analogues

Excess of the electrophilic reagents converted the starting cluster **1** to monomers as shown in Fig. 1 and 2. In the case of iodo-acetonitrile the new 18 electron Pt(II) complex $[\text{Pt}(\text{CO})(\text{PCy}_3)(\text{CH}_2\text{CN})]$ (**5**) was observed. This complex is barely soluble in toluene, thus the pure product could be separated from the solution as an ivory solid. X-Ray analysis (an ORTEP representation is shown in Fig. 14) showed that **5** is a square planar platinum complex which has a *trans* CO- CH_2CN arrangement (selected bond lengths and angles are listed in Table 11). The Pt-P, Pt-C(carbonyl) and Pt-I distances are within the usual ranges. Due to the larger steric demand of the cyclohexyl group compared to phenyl, the Pt-C2 value of 2.181 Å is longer than the corresponding bond lengths (2.121 Å) observed in *cis*- $[\text{Pt}(\text{CH}_2\text{CN})_2(\text{PPh}_3)]$.⁴⁷

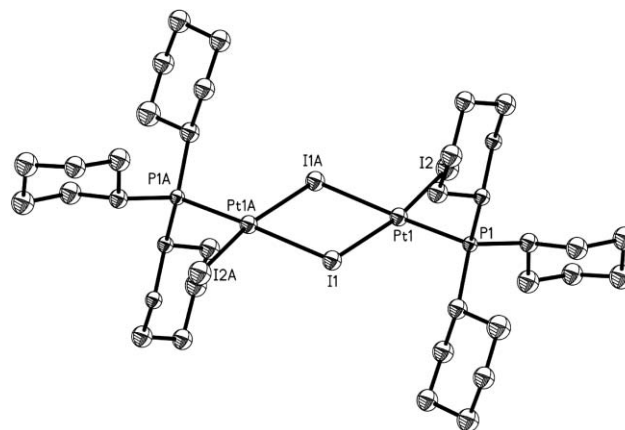
NMR and IR spectroscopic measurements showed that stereochemistries in solution and in the solid state are similar. The ^{31}P and ^{13}C NMR spectra show one phosphine ($\delta = 28.7$ ppm) and one carbonyl (173.5 ppm) environment, with the expected satellites due to coupling with one ^{195}Pt nuclei (3179 and 1120 Hz, respectively). The magnitude of the $^2J(\text{C-P})$ coupling constant (5.9 Hz) confirmed the *cis* arrangement of CO and PCy_3 ligands. The ^{195}Pt spectrum of the 100% ^{13}C labelled complex **5** showed a

**Fig. 14** ORTEP view of monomer **5**.**Table 11** Important bond lengths (Å) and angles (°) in **5**

Pt1-P1	2.298(3)	Pt1-I1	2.648(12)
Pt1-C2	2.181(12)	Pt1-C1	1.919(16)
I1-Pt1-P1	178.24(9)	C2-Pt1-I1	85.9(4)
C1-Pt1-I1	84.6(4)	C1-Pt1-C2	169.9(5)

doublet of doublet centered at -4738 ppm, a value in the typical chemical shift range for Pt(II) complexes.

Elemental halogens converted **1** to monomers *cis*- $[\text{PtX}_2(\text{CO})(\text{PCy}_3)]$ (X = I, **6a** and Br, **6b**). These types of complexes with different tertiary phosphines are well known from the literature.^{18,19,23,48-52} X-ray analyses of *cis*- $[\text{PtBr}_2(\text{CO})\text{PCy}_3]$ (**6b**) and $[\text{Pt}(\text{I})(\text{CO})\text{PCy}_3]$ (**6c**) has been undertaken (see supplementary crystallographic data). The X-ray structure of the known¹⁶⁻²³ Pt(II) dimer $[\text{Pt}_2(\mu\text{-I})_2(\text{PCy}_3)_2]$ **8** (an ORTEP representation is shown in Fig. 15) which is a fragmentation product of **7a** has been determined as well.

**Fig. 15** ORTEP (50% probability level) representation of **8**.

Conclusions

The formation of a Pt–alkyl bond by oxidative addition to a platinum cluster compound is not documented. We found that the oxidative addition of iodo-acetonitrile to $[\text{Pt}_3(\mu\text{-CO})_3(\text{PCy}_3)_3]$ in equimolar ratio gives the adduct $[\text{Pt}_3(\mu\text{-CO})_3(\text{PCy}_3)_3\text{I}(\text{CH}_2\text{CN})]$ (**2**) where one Pt atom is inserted into the I–CH₂CN bond. The reaction, however, is more complicated when excess of iodo-acetonitrile is added to the starting cluster, as fragmentation to dimers such as $[\text{Pt}_2(\text{CO})_2(\text{PCy}_3)_2\text{I}(\text{CH}_2\text{CN})]$ (**3**) and monomers takes place. Since one monomer *cis*- $[\text{PtI}_2(\text{CO})(\text{PCy}_3)]$ and succinonitrile are formed, the fragmentation must take place partly by homolytic scission of the Pt–CH₂CN bond.

Oxidative addition of iodine to $[\text{Pt}_3(\mu\text{-CO})_3(\text{PCy}_3)_3]$ resembles that of iodo-acetonitrile in the sense that an adduct is formed when using 1 : 1 mole ratio of reactant, *i.e.* $[\text{Pt}_3(\mu\text{-CO})_2(\mu\text{-I})\text{I}(\text{PCy}_3)_3]$ where one platinum atom inserted into the I–I bond as it is does into the I–CH₂CN bond giving $[\text{Pt}_3(\mu\text{-CO})_3\text{I}(\text{CH}_2\text{CN})(\text{PCy}_3)_3]$. In the former case, insertion was followed by CO substitution by I[−], as iodide can have two binding modes (terminal and bridging), whereas in the latter case the –CH₂CN group can only be terminal and no CO substitution can occur. A complicated fragmentation is observed in the presence of excess of elemental iodine (or bromine) giving monomers as final products and dimers such as $[\text{Pt}_2(\text{CO})_2\text{I}_2(\text{PCy}_3)_2]$ as intermediates. The crystal structure of the latter indicated that the dimer is chiral with all ligands being terminally bonded. The existence of enantiomers in solution could not be established with certainty when trying to replace the iodide ligand with an NMR active atom as structural indicator *i.e.* when reacting the dimer with SnCl₂ (to give Pt–SnCl₂I), it was found that SnCl₂ inserted into the metal–metal bond giving the new compound $[\text{Pt}_2(\mu\text{-SnCl}_2)(\text{CO})_2(\text{PCy}_3)_2\text{I}_2]$ which evidently is not chiral.

Experimental

All manipulations were carried out under a nitrogen atmosphere using standard Schlenk techniques. All solvents were dried and distilled prior to use. Infrared spectra (CaF₂ cells) were recorded on a Perkin–Elmer 983 spectrometer, and NMR spectra on Bruker AC 200 (¹H at 200.13 MHz, ³¹P at 81.02 MHz and ¹³C at 50.32 MHz), Bruker WH 360 (¹³C at 90.55 MHz) and Bruker DRX 400 (³¹P at 161.93 MHz, ¹³C at 100.6 MHz and ¹⁹⁵Pt at 84.5 MHz) spectrometers. The chemical shifts (δ) are referred to external TMS (¹H and ¹³C) external 85% H₃PO₄ (³¹P), and Na₂PtCl₆ (¹⁹⁵Pt). The spectra of all nuclei were ¹H decoupled. Simulations were performed with the gNMR 4.1 program, considering only the relative populations of platinum isotopomers since all samples for ¹³C{¹H} NMR were enriched to $\geq 99\%$ ¹³CO. $[\text{Pt}_3(\text{CO})_3(\text{PCy}_3)_3]$ was prepared by the literature method.⁵³ The ¹³C isotopically labelled derivative was prepared similarly, using ¹³CO enriched to 99%. Iodo-acetonitrile, I₂, Br₂, NaBEt₃H, SnCl₂·2H₂O (Aldrich) and carbon monoxide ($>99\%$ ¹³CO) were used as received (Aldrich).

The relevant details of the crystal, data collection, and structural refinement are listed in the supplementary crystallographic data. Diffraction data were collected using Mo K α radiation. The structure was refined using the full-matrix least-squares on *F*². All structures have been refined anisotropically, except **2** and **7a** for which light atoms (C, N and O) have unstable behaviour and then retained isotropic. The same problem occurred in the refinement of compound **8a** for which also P and Cl atoms have been retained isotropic. Isotropic is also the refinement of a disordered solvent molecule in the crystal structure of compound **4a**. All hydrogens were made to ride isotropically on their associated carbons. Structure refinement and geometrical calculations were carried out on all structures with the SHELXL-97.⁵⁴ Graphical representations of the molecular structures in the crystal were generated with the program ORTEP.⁵⁵

Syntheses

[Pt₃I(CH₂CN)(μ-CO)₃(PCy₃)₃] (2). A solution of $[\text{Pt}_3(\mu\text{-CO})_3(\text{Cy}_3)_3]$ (0.29 g, 0.19 mmol) in toluene (25 ml) was cooled to -70°C in a N₂(l)/acetone bath and ICH₂CN (14 μl, 0.19 mmol) was added with a Hamilton syringe. The mixture was stirred for 30 min, 10 min at -50°C and 10 min at -20°C . The solvent was evaporated to dryness at this temperature over a period of 3 h. The product is a mixture of **2** and **3**. Single crystals were obtained from a toluene solution of this mixture by slow diffusion of ethanol. IR and NMR data: Table 3. X-Ray data: see Table 1, Table 12 and supplementary crystallographic data.

[Pt₂I(CO)₂(PCy₃)₂(CH₂CN)] (3). A solution of $[\text{Pt}_3(\mu\text{-CO})_3(\text{Cy}_3)_3]$ (0.29 g, 0.19 mmol) in toluene (25 ml) was cooled to -50°C in N₂(l)/acetone bath and ICH₂CN (21 μl, 0.29 mmol) was added with a Hamilton syringe. The mixture was stirred for 20 min, for another 10 min at -20 and 0°C and finally for 1 h at room temperature. Concentration of the resulting solution gave a red–brown solid. (Yield: 0.245 g, 72%). An analytically pure sample could not be obtained. Selected IR data (cm^{−1}): toluene solution $\nu(\text{C}\equiv\text{O})$ 2007; 2035vs; $\nu(\text{C}\equiv\text{N})$ 2205 m. NMR data: see Table 5.

[PtI(CO)(PCy₃)(CH₂CN)] (5). A solution of $[\text{Pt}_3(\mu\text{-CO})_3(\text{Cy}_3)_3]$ (0.29 g, 0.19 mmol) in toluene (25 ml) was cooled to -20°C in N₂(l)/acetone bath and ICH₂CN (45 μl, 0.62 mmol) was added. The mixture was stirred for 10 min in the cold, for another 10 min at 0°C , and finally for a night at room temperature. Filtration of the concentrated toluene solution resulted in a whitish-yellow solid, which could be recrystallized from dichloromethane/heptane mixture. (Yield: 0.220 g, 57.2%). Selected IR data (cm^{−1}): in THF solution $\nu(\text{C}\equiv\text{O})$ 2080vs; $\nu(\text{C}\equiv\text{N})$ 2214w. Anal. Calc. for C₂₁H₃₅INOPPt: C, 37.62; H, 5.26; N, 2.09. Found: C, 37.57; H, 5.31; N, 2.05. NMR data: see text. Crystal data of **5**: see supplementary crystallographic data and Table 12.

Evidence for the formation of succinonitrile

A THF solution of **3** was magnetically stirred for one day at 60°C under N₂. The solvent was evaporated at reduced pressure. A MeOH extract of the product was analyzed by GC-MS with a source temperature of 150°C . Characteristic *m/z* were found at 81 (34.4%), 53 (100%), which were consistent with the spectral features presented in the GC-MS spectrum of a MeOH solution of succinonitrile recorded under the same conditions (*m/z*: 81 (20.9), 53 (100)). A third measurement was made on a MeOH solution of ICH₂CN to exclude the direct formation of succinonitrile under the measurement conditions. The *m/z* lines found in the latter spectrum are: 167 (81.38), 144 (100), 127 (16.48). The IR spectrum shows a CN band at 2254 cm^{−1}.

[Pt₂I₂(CO)₂(PCy₃)₂] (4a). A THF solution (25 ml) of $[\text{Pt}_3(\mu\text{-CO})_3(\text{PCy}_3)_3]$ (0.20 g, 0.124 mmol) was cooled to -60°C in a N₂(l)/EtOH bath and I₂ (dissolved in 5 ml toluene, 51 mg, 0.2 mmol) was added with a syringe. The mixture was stirred for 10 min at low temperature, for another 10 min at 0°C and finally for a short time at room temperature. Partial evaporation of solvent and addition of MeOH to the solution gave a yellow–brown solid. (Yield: 0.130g, 55%). Selected IR data (cm^{−1}): THF solution $\nu(\text{C}\equiv\text{O})$ 2031vs; 2010vs. Anal. Calc. for C₃₈H₆₆I₂O₂Pt₂: C, 36.20; H, 5.28. Found: C, 35.70; H, 5.46. Yellow single crystals were grown from toluene at 5°C in a 10 mm NMR tube over 2 months. NMR data: see Table 6. X-Ray data: see Table 7, Table 12 and supplementary crystallographic data.

[Pt₂Br₂(CO)₂(PCy₃)₂] (4b). As for **4a** starting from **1** (0.2 g, 0.124 mmol) and treated with Br₂ (10 μl, 0.129 mmol). Yellow–brown solid, 0.130 g (60%). IR (cm^{−1}): THF solution $\nu(\text{C}\equiv\text{O})$ 2032; 2012vs. Anal. Calc. for Br₂C₃₈H₆₆O₂Pt₂: C, 39.11; H, 5.70. Found: C, 39.28; H, 5.60. NMR data: see Table 6.

Table 12 Crystal data and details of the structure determination for: **2**, **4a**, **5**, **6b**, **6c**, **7a**, **8a** and **9a**

	2	4a	5	6b	6c	7a	8	9a	
Empirical formula	C _{83.50} H ₁₂₉ INO ₃ P ₃ Pt ₃	C _{62.50} H ₉₄ I ₂ O ₂ P ₂ Pt ₂	C ₂₁ H ₃₅ INO ₃ Pt	C ₁₉ H ₃₃ Br ₂ OPt	C ₁₉ H ₃₃ ClO ₃ Pt	C ₆₃ H ₁₀₇ I ₂ O ₂ P ₃ Pt ₃	C ₃₈ H ₇₀ Cl ₁₄ P ₂ Pt ₂	C ₄₀ H ₇₀ Cl ₁₆ O ₂ P ₂ Pt ₂ Sn	
Formula weight	1999.96	1583.3	670.46	663.33	665.33	1828.47	1628.46	1620.27	
Temperature	140(2) K	140(2) K	140(2) K	140(2) K	140(2) K	140(2) K	140(2) K	140(2) K	
Wavelength	0.71073 Å	0.71070 Å	0.71070 Å	0.71073 Å	0.71070 Å	0.71073 Å	0.71073 Å	0.71070 Å	
Crystal system	Triclinic	Triclinic	Monoclinic	Orthorhombic	Monoclinic	Triclinic	Triclinic	Triclinic	
Space group	P-1	P1	P2(1)/c	Pnma	P2(1)/n	P1	P1	P-1	
Unit cell dimensions	<i>a</i> = 14.1422(8) Å <i>b</i> = 14.212(18) Å <i>c</i> = 23.2836(9) Å <i>α</i> = 90° <i>β</i> = 14.212(18) Å <i>γ</i> = 90°	<i>a</i> = 12.631(2) Å <i>b</i> = 16.054(12) Å <i>c</i> = 97.406(13) Å <i>α</i> = 90° <i>β</i> = 16.054(12) Å <i>γ</i> = 90°	<i>a</i> = 9.502(3) Å <i>b</i> = 12.714(4) Å <i>c</i> = 91.247(18) Å <i>α</i> = 90° <i>β</i> = 12.714(4) Å <i>γ</i> = 90°	<i>a</i> = 14.0408(8) Å <i>b</i> = 16.8481(10) Å <i>c</i> = 9.3995(5) Å <i>α</i> = 90° <i>β</i> = 90° <i>γ</i> = 90°	<i>a</i> = 10.750(2) Å <i>b</i> = 13.4635(6) Å <i>c</i> = 90.668(16) Å <i>α</i> = 90° <i>β</i> = 13.4635(6) Å <i>γ</i> = 90°	<i>a</i> = 10.4474(4) Å <i>b</i> = 14.1666(9) Å <i>c</i> = 23.8599(12) Å <i>α</i> = 90° <i>β</i> = 14.1666(9) Å <i>γ</i> = 90°	<i>a</i> = 10.040(3) Å <i>b</i> = 86.73(2)° <i>c</i> = 74.46(3)° <i>α</i> = 10.040(3) Å <i>β</i> = 74.46(3)° <i>γ</i> = 63.32(3)°	<i>a</i> = 10.040(3) Å <i>b</i> = 86.73(2)° <i>c</i> = 74.46(3)° <i>α</i> = 10.040(3) Å <i>β</i> = 74.46(3)° <i>γ</i> = 63.32(3)°	<i>a</i> = 11.857(5) Å <i>b</i> = 86.04(4)° <i>c</i> = 13.136(10) Å <i>α</i> = 11.857(5) Å <i>β</i> = 86.04(4)° <i>γ</i> = 75.72(5)°
Volume/Å ³	4044.5(4)	3201.3(7)	2279.1(11)	2223.6(2)	2227.8(6)	3389.7(3)	1189.7(6)	2718(3)	
Z	2	2	4	4	4	2	1	2	
<i>D</i> _{calc} (Mg m ⁻³)	1.642	1.643	1.954	1.981	1.985	1.791	2.273	1.980	
<i>μ</i> (mm ⁻¹)	5.663	5.418	7.592	9.981	7.880	7.195	8.786	7.109	
<i>F</i> (000)	1986	1554	1288	1272	1272	1772	764	1540	
Reflections collected	24446	20804	13172	12489	13521	20350	7030	17683	
Independent reflections	12541	10600	4000	2029	3832	10528	3693	9006	
Data/restraints/parameters	12541/9/423	10600/5/653	4000/0/236	2029/2/125	3832/0/218	10528/0/333	3693/0/116	9006/0/496	
<i>R</i> ^a [<i>I</i> > 2σ(<i>I</i>)]	0.0489	0.0416	0.0676	0.0446	0.0397	0.0509	0.1024	0.1260	
<i>wR</i> ² (all data)	0.1386	0.1193	0.0984	0.0984	0.1144	0.1533	0.2838	0.3586	
GoF ^b	0.989	1.063	1.112	1.187	1.128	1.074	1.067	1.098	
Largest diff. peak and hole/e Å ⁻³	5.595 and -1.581	1.443 and -1.835	1.691 and -2.511	1.567 and -1.603	2.011 and -1.913	2.289 and -3.137	11.930 and -5.112	5.931 and -3.927	

^a $R = \sum ||F_o| - |F_c|| / \sum |F_o|$, $wR2 = \{ \sum [w(F_o^2 - F_c^2)]^2 / \sum [w(F_o^2)] \}^{1/2}$; ^b $GoF = \{ \sum [w(F_o^2 - F_c^2)]^2 / (n - p) \}^{1/2}$ where *n* is the number of data and *p* is the number of parameters refined.

[Pt₂Cl₂(CO)₂(PCy₃)₂] (**4c**). This complex was prepared following the method reported by Mingos *et al.*²⁴ for [Pt₂Cl₂(CO)₂(PNpPh₂)₂] starting with [PtCl₂(COD)] (0.3 g, 0.8 mmol). Yield 0.218 g (51%) as brown microcrystals. An analytically pure sample could not be obtained as it contained small amounts of **1** and **6**. NMR data: see Table 6.

[PtI₂(CO)PCy₃] (**6a**), [PtBr₂(CO)PCy₃] (**6b**) and [PtCl(I)(CO)PCy₃] (**6c**). Complex **6a** was prepared following the literature method.¹⁹ **6b** and **6c** were obtained as minor products in the preparation of **4b** and **9a**, respectively. X-Ray data for the latter two complexes: see supplementary crystallographic data and Table 12.

Pt₃I(μ-I)(μ-CO)₂(PCy₃)₃] (**7a**). A toluene solution (25 ml) of [Pt₃(μ-CO)₃(PCy₃)₃] (0.10 g, 0.062 mmol) was cooled to -60 °C in a N₂(l)/EtOH bath and I₂ (dissolved in 5 ml toluene, 17 mg, 0.066 mmol) was added with a syringe. The mixture was stirred for 10 min at low temperature, for another 10 min at 0 °C and finally for a short time at room temperature. A mixture of **7a** and **4a** was formed. The mixture was separated on a 20 × 20 mm TLC plate (Kieselgel 60 F₂₅₄). Elution with dichloromethane/hexane 1 : 2 gave a dark red band following a yellow band of **4a** (yield: 20 mg, 17.4%). Anal. Calc. for C₅₆H₉₀I₂O₂P₃Pt₃: C, 38.74; H, 5.75. Found: C, 39.18; H, 5.90. Selected IR data (cm⁻¹): THF solution ν(C≡O) 2066vs and 2042sh. NMR data: see Table 4. Dark red single crystals were obtained from THF solution of the mixture of **7a** and **4a** at -20 °C with slow diffusion of heptane. X-Ray data: see Table 2, Table 12 and supplementary crystallographic data.

[Pt₂Br(μ-Br)(μ-CO)₂(PCy₃)₃] (**7b**). As for **7a** using Br₂ instead of I₂. No attempts to separate the mixture of **7b** and **4b** were made. NMR data: see Table 4.

[Pt₂I₂(μ-I)₂(PCy₃)₂] (**8**). This complex was prepared following the method reported by Al-Najjar.¹⁹ Yellow single crystals were obtained from a CH₂Cl₂ solution standing at -20 °C with the formula [Pt₂I₂(μ-I)₂(PCy₃)₂]·2CH₂Cl₂. X-Ray data: see supplementary crystallographic data and Table 12.

[Pt₂I₂(SnCl₂)(CO)₂(PCy₃)₂] (**9a**). SnCl₂·2H₂O (0.013 g, 0.576 mmol) was suspended in a CH₂Cl₂ solution of **4a** (0.070 g, 0.55 mmol) and vigorously stirred for 10 min. The reaction progress was monitored by IR (disappearance of ν(C≡O) at 2031vs and 2010vs, and appearance of ν(C≡O) at 2058 cm⁻¹). Addition of MeOH following concentration of the resulting solution gave a yellow solid. (Yield: 0.060 g, 73%). Slow diffusion of MeOH into a dichloromethane solution at -20 °C gives yellow crystals. Anal. Calc. for C₃₈Cl₂H₆₆I₂O₂P₂Pt₂Sn: C, 31.47; H, 4.58. Found: C, 31.23; H, 4.69. NMR data: see Table 8. A supplementary structure is available with a bad *R* factor (see supplementary crystallographic data and Table 12).

[Pt₂Cl₂(SnCl₂)(CO)₂(PCy₃)₂] (**9c**). As for **9a** starting from **4c**. Analytically pure sample could not be obtained due to decomposition. NMR data: see Table 8.

CCDC reference numbers 246661–246668.

See <http://www.rsc.org/suppdata/dt/b4/b415311a/> for crystallographic data in CIF or other electronic format.

DFT calculations

All computations were carried out with the Amsterdam Density Functional (ADF) software package.^{56–58} The computation of nuclear coupling constants employed the *cpI* code implemented by Autsbach and Ziegler,^{59,60} which calculates analytically nuclear spin–spin coupling constants based on the relativistic zero-order regular approximation (ZORA).^{61,62} The Vosko–Wilk–Nusair (VWN)⁶³ local density functional and the Becke–Lee–Yang–Parr^{64–67} exchange and correlation functional have been used for geometry optimization. As basis sets ZORA/TZ2P were used for all elements.⁵⁸ Electrons in the lower shells either

were (frozen core: Pt-4f, C-1s, O-1s, N-1s, Cl-2p, I-4p) or were not (full electron) treated with the frozen core approximation.

Preliminary calculations on the model systems containing PH_3 as ligand have shown that coupling constants are dominated by the scalar relativistic Fermi contact (FC) term while the other three, *i.e.* spin-dipole (SD), paramagnetic orbital (OP), and diamagnetic orbital (OD) terms, were found to be relatively negligible. Based on this observation, only the FC term was calculated for the larger systems (PMe_3).

References

- R. A. Periana, D. J. Taube, S. Gamble, H. Taube, T. Satoh and H. Fujii, *Science*, 1998, **280**, 560.
- T. M. Gilbert, I. Hristov and T. Ziegler, *Organometallics*, 2001, **20**, 1183.
- S. Sakaki, B. Biswas, and M. Sugimoto, *J. Chem. Soc., Dalton Trans.*, 1997.
- J. P. Collman, L. S. Hegedus, J. R. Norton, and R. G. Finke, *Principles and Applications of Organotransition Metal Chemistry*, Oxford University Press, 1987.
- M. C. Jennings and R. J. Puddephatt, *Inorg. Chem.*, 1988, **27**, 4280.
- G. J. Spivak, L. Hao, J. J. Vittal and R. J. Puddephatt, *J. Am. Chem. Soc.*, 1996, **118**, 225.
- L. Hao, L. Manojlovic-Muir, K. W. Muir, R. J. Puddephatt, G. J. Spivak, J. J. Vittal and D. Yuffitt, *Inorg. Chim. Acta*, 1997, **265**, 65.
- Z. Beni, R. Scopelliti and R. Roulet, *Inorg. Chem. Commun.*, 2004, **7/8**, 935.
- R. Ros, A. Tassan, R. Roulet, G. Laurency, V. Duprez and K. Schenk, *J. Chem. Soc., Dalton Trans.*, 2002, 3565.
- R. Ros, A. Tassan, R. Roulet, V. Duprez, S. Detti, G. Laurency and K. Schenk, *J. Chem. Soc., Dalton Trans.*, 2001, 2858.
- R. Ros, A. Tassan, G. Laurency and R. Roulet, *Inorg. Chim. Acta*, 2000, **303**, 94.
- R. Ros, G. Facchin, A. Tassan, R. Roulet, G. Laurency and F. Lukacs, *J. Cluster Sci.*, 2001, **12**, 99.
- A. S. Goel and S. Goel, *Inorg. Nucl. Chem. Lett.*, 1980, **16**, 397.
- C. Couture, D. H. Farrar, D. S. Fisher and R. R. Gukathasan, *Organometallics*, 1987, **6**, 532.
- J. Autsbach, D. I. Ciprian and T. Ziegler, *J. Am. Chem. Soc.*, 2003, **125**, 1028.
- M. Black, R. H. B. Mais and P. G. Owston, *Acta Crystallogr., Sect. B*, 1969, **25**, 1760.
- S. F. Watkins, *J. Am. Chem. Soc. A*, 1970, 168.
- G. K. Anderson, H. C. Clark and J. A. Davis, *Organometallics*, 1982, **1**, 550.
- I. M. Al-Najjar, *Inorg. Chim. Acta*, 1987, **128**, 93.
- B. L. Simms, M. Shang, J. Lu, W. J. Youngs and J. A. Ibers, *Organometallics*, 1987, **6**, 1118.
- A. J. Blake, R. O. Gould, A. M. Marr, D. W. H. Rankin and M. Schroder, *Acta Crystallogr., Sect. C*, 1989, **45**, 1218.
- N. M. Boag and M. S. Ravetz, *Acta Crystallogr., Sect. C*, 1996, **52**, 1942.
- G. K. Anderson and R. J. Cross, *J. Chem. Soc., Dalton Trans.*, 1980, 1988.
- T. E. Müller, F. Ingold, S. Menzer, D. M. P. Mingos and D. J. Williams, *J. Organomet. Chem.*, 1997, **528**, 163.
- A. Albinati, G. Carturan and A. Musco, *Inorg. Chim. Acta*, 1976, **16**, L3.
- A. Albinati, *Inorg. Chim. Acta*, 1977, **22**, L31.
- D. J. Underwood, R. Hoffman, K. Tatsuni, A. Nakamura and Y. Yamamoto, *J. Am. Chem. Soc.*, 1985, **107**, 5968.
- D. M. P. Mingos and T. Slee, *J. Organomet. Chem.*, 1990, **394**, 679.
- A. Moor, P. S. Pregosin and L. M. Venanzi, *Inorg. Chim. Acta*, 1981, **48**, 153.
- C. E. Briant, D. L. Gilmour and D. M. P. Mingos, *J. Organomet. Chem.*, 1986, **308**, 381.
- P. S. Pregosin, *Annu. Rep. NMR Spectrosc.*, 1986, **17**, 285.
- C. S. Brownings and D. H. Farrar, *Organometallics*, 1989, **8**, 813.
- A. Albinati, K.-H. Dahmen, F. Demartin, J. F. Forward, C. J. Longley, D. M. P. Mingos and L. M. Venanzi, *J. Chem. Soc., Chem. Commun.*, 1992, 924.
- A. Dedieu and R. Hoffman, *J. Am. Chem. Soc.*, 1978, **100**, 2074.
- R. J. Goodfellow, P. L. Goggin and L. M. Venanzi, *J. Chem. Soc. A*, 1967, 1897.
- D. Adams, P. J. Chandler and R. G. Churchill, *J. Chem. Soc. A*, 1967, 1072.
- N. M. Boag, P. L. Goggin, R. J. Goodfellow and I. R. Herbert, *J. Chem. Soc., Dalton Trans.*, 1983, 1101.
- R. J. Goodfellow and I. R. Herbert, *Inorg. Chim. Acta*, 1982, **65**, L161.
- G. W. Bushnell, D. T. Eadie, A. Pidcock, A. R. Sam, R. D. Holmes-Smith and S. R. Stobart, *J. Am. Chem. Soc.*, 1982, **104**, 5837.
- M. C. Janzen, M. C. Jennings and R. J. Puddephatt, *Organometallics*, 2001, **20**, 4100.
- P. S. Pregosin and H. Rueger, *Inorg. Chim. Acta*, 1984, **86**, 55.
- M. Green, J. A. K. Howard, M. Murray, J. L. Spencer and F. G. A. Stone, *J. Chem. Soc., Dalton Trans.*, 1977, 1509.
- J. Autsbach and B. Le Guennic, *J. Am. Chem. Soc.*, 2003, **125**, 13585.
- A. Klamt, *J. Phys. Chem.*, 1995, **99**, 2224.
- A. Klamt and V. Jones, *J. Chem. Phys.*, 1996, **105**, 9972.
- A. Klamt and G. Schuurmann, *J. Chem. Soc., Perkin Trans.*, 1993, **2**, 799.
- W. Henderson and A. G. Oliver, *Acta Crystallogr., Sect. C*, 1999, **C55(9)**, 1408.
- C. Y. Mok, S. G. Tan and G. C. Chan, *Inorg. Chim. Acta*, 1990, **176**, 43.
- D. G. Evans, M. F. Hallam, D. M. P. Mingos and R. W. M. Wardle, *J. Chem. Soc., Dalton Trans.*, 1987, 1889.
- H. C. Clark, A. S. Goel and C. S. Wong, *Inorg. Chim. Acta*, 1979, **34**, 159.
- L. Manojlovic-Muir, K. W. Muir and R. Walker, *J. Chem. Soc., Dalton Trans.*, 1976, 1379.
- L. Manojlovic-Muir, K. W. Muir and T. Solomun, *J. Organomet. Chem.*, 1977, **142**, 265.
- K.-H. Dahmen, A. Moor, R. Naegeli and L. M. Venanzi, *Inorg. Chem.*, 1991, **30**, 4285.
- G. M. Sheldrick, *SHELXL-97*, Institut für Anorganische Chemie der Universität, Tmmanstarse 4, D-3400 Göttingen, Germany, 1997..
- L. J. Faruggia, *Appl. Crystallogr.*, 1997, **30**, 565.
- C. Fonseca Guerra, O. Visser, J. G. Snijders, G. te Velde, and E. J. Baerends, in *Parallelization of the Amsterdam Density Functional Program*, Cagliari, 1995.
- G. te Velde, F. M. Bickelhaupt, E. J. Baerends, S. J. A. van Gisbergen, C. Fonseca Guerra, J. G. Snijders and T. Ziegler, *J. Comput. Chem.*, 2001, **22**, 931.
- ADF, Amsterdam Density Functional, Theoretical Chemistry*, Vrije Universiteit, Amsterdam..
- J. Autsbach and T. Ziegler, *J. Chem. Phys.*, 2000, **113**, 9410.
- J. Autsbach and T. Ziegler, *J. Chem. Phys.*, 2000, **113**, 936.
- E. van Lenthe, E. J. Baerends and J. G. Snijders, *J. Chem. Phys.*, 1993, **99**, 4597.
- E. van Lenthe, *The ZORA equation*, Vrije Universiteit, Amsterdam, 1996..
- S. H. Vosko, L. Wilk and M. Nusair, *Can. J. Phys.*, 1989, **58**, 1200.
- A. D. Becke, *Phys. Rev. A*, 1988, **38**, 3098.
- C. Lee, W. Yang and R. G. Parr, *Phys. Rev. B*, 1988, **37**, 785.
- B. G. Johnson, P. M. W. Gill and J. A. Pople, *J. Chem. Phys.*, 1993, **98**, 5612.
- T. V. Russo, R. L. Martin and P. J. Hay, *J. Chem. Phys.*, 1994, **101**, 7729.